JOURNAL OF COMPUTATIONAL PHYSICS 106, 92–100 (1993)

High Order Finite Difference and Multigrid Methods for Spatially Evolving Instability in a Planar Channel*

C. LIU AND Z. LIU

Computational Mathematics Group, University of Colorado at Denver, Campus Box 170, P.O. Box 173364, Denver, Colorado 80217-3364

Received November 26, 1991; revised June 19, 1992

A computational study of the spatial instability of planar Poiseuille flow is presented. A fourth-order finite difference with a fully implicit time-marching scheme is developed on a staggered grid. A semi-coarsening multigrid method is applied to accelerate convergence for the implicit scheme at each time step and a line distributive relaxation is developed as a fast solver, which is very robust and efficient for anisotropic grids. A new treatment for outflow boundary conditions makes the buffer area as short as one wavelength. The computational results demonstrate high accuracy in terms of agreement with linear theory and excellent efficiency in the sense that cost is comparable to (and usually less than) explicit schemes. © 1993 Academic Press, Inc.

1. INTRODUCTION

Developing an understanding of flow transition at high Reynolds number has been a central problem in the theory of fluid motion for over a century. It also has great practical interest. The present work was motivated by the need to develop efficient and accurate Navier–Stokes solvers for spatially evolving stability and transition problems in wall-bounded flows. An computationally efficient *temporal* approach [1], which follows the time evolution of a single wavelength of the disturbance, has been widely applied to simulate the transition process. A very efficient multigrid finite volume scheme has been developed by C. Liu *et al.* (cf. [2–4]) that achieves very good agreement with linear theory for temporal evolution induced by small disturbances. However, the temporal model requires the assumption of streamwise periodicity and approximate parallel flow, which is unrealistic in the case of boundary layers. Therefore, as transition in channel and boundary layer flow is evolving in the streamwise direction, it is natural to simulate this process with a *spatial* approach that incorporates a more realistic-sized channel. The present work uses multigrid methods and high-order differences to simulate spatially evolving flows in a planar channel.

The accurate Navier–Stokes solver for tracking the spatial evolution of a disturbance field has several requirements:

- phase-accurate discretization of the convective terms
- high resolution for regions close to the solid wall
- correct outflow boundary conditions that remain nonreflective even in the presence of nonlinear wave interaction.

The first two requirements can be met by use of high-order finite differences and fully implicit time-marching, and the third by using a buffer domain [5] in which a modification to the Navier–Stokes equations is used. A buffer domain is an effective method for treating the outflow boundary conditions, but only if the buffer domain is kept to a minimum size. The present work gives a new specification for the outflow boundary condition on a staggered grid that uses a buffer domain which can be shorter than one wavelength, without any induced reflection in the physical domain.

As in our earlier work, the multigrid method based on distributive relaxation [6] is applied for accelerating the convergence process. Since the grid used for channel flow is highly anisotropic, a semi-coarsening multigrid algorithm based on line distributive relaxation is developed to achieve optimal multigrid efficiency.

2. GOVERNING EQUATIONS AND LINEAR SOLUTIONS

The two-dimensional, time-dependent, incompressible Navier–Stokes equations, which are nondimensionized by the channel half height, h and the centerline velocity, U, are considered as the governing equations for planar channel flow (Fig. 1):

$$\frac{\partial u}{\partial t}+\frac{\partial uu}{\partial x}+\frac{\partial uv}{\partial y}-\frac{1}{\mathrm{Re}}\left(\frac{\partial^2 u}{\partial x^2}+\frac{\partial^2 u}{\partial y^2}\right)+\frac{\partial P}{\partial x}=0, \tag{1}$$

$$\frac{\partial v}{\partial t}+\frac{\partial uv}{\partial x}+\frac{\partial vv}{\partial y}-\frac{1}{\mathrm{Re}}\left(\frac{\partial^2 v}{\partial x^2}+\frac{\partial^2 v}{\partial y^2}\right)+\frac{\partial P}{\partial y}=0, \tag{2}$$

$$\frac{\partial u}{\partial x}+\frac{\partial v}{\partial y}=0, \tag{3}$$

* This work was supported by NASA under Grant NAS1-19016.

0021-9991/93 $5.00

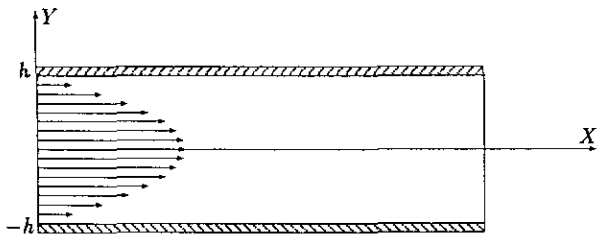

FIG. 1. Planar channel flow.

where u and v are velocity components in the x- and y-directions, respectively; P is the pressure; and Re is the Reynolds number based on the centerline velocity U of mean flow, channel half-width h, and viscous parameter ν:

$$\mathrm{Re} = Uh/\nu. \tag{4}$$

In Eqs. (1)–(3), the velocity vector and pressure, respectively, can be decomposed into their means, $\mathbf{V}_0$ and P_0, and fluctuating parts, $\mathbf{V}'$ and P',

$$\begin{aligned} \mathbf{V} &= \mathbf{V}_0(x, y) + \mathbf{V}'(x, y, t), \\ P &= P_0 + P'. \end{aligned} \tag{5}$$

Here, $\mathbf{V}_0$ and P_0 are based on Poiseuille flow:

$$\begin{aligned} \mathbf{V}_0(x, y) &= (1 - y^2, 0), \\ P_0 &= -\frac{2}{\mathrm{Re}}\, x + \text{const.} \end{aligned} \tag{6}$$

Using the above notation, the boundary conditions can be described as

$$\begin{aligned} &\mathbf{V}(x, y = \pm 1, t) = 0, \\ &\mathbf{V}_0(x = 0, y) = (1 - y^2, 0), \\ &\mathbf{V}'(x = 0, y, t) = \varepsilon\, \mathrm{Real}\{\mathbf{V}_{\mathrm{se}}(y)\, e^{-i\omega_R t}\}, \end{aligned} \tag{7}$$

where ε is the amplitude of the perturbation velocities; $\mathbf{V}_{\mathrm{se}}$ is the complex velocity vector calculated from the spatial eigenfunction of the Orr–Sommerfeld equation corresponding to the real frequency, ω_R; $i = \sqrt{-1}$; and *Real* stands for the real part of a complex number. The outflow boundary conditions are not given here but will be discussed later in this paper.

For small ε, the linear theory (Orr–Sommerfeld equation) provides a solution to the governing equations, which can be written as

$$\mathbf{V}' = \varepsilon e^{-\alpha_I x}\, \mathrm{Real}\{\mathbf{V}_{\mathrm{se}}(y)\, e^{i(\alpha_R x - \omega_R t)}\}, \tag{8}$$

where $\alpha = \alpha_R + i\alpha_I$ is the least damped spatial eigenvalue of the Orr–Sommerfeld equation for a given Re and ω_R.

The Orr–Sommerfeld equation that governs the linear stability of parallel shear flow may be written as

$$\left[\left(\frac{d^2}{dy^2} - \alpha^2\right)^2 - i\,\mathrm{Re}\left\{(\alpha u_0 - \omega_R)\left(\frac{d^2}{dy^2} - \alpha^2\right) - \alpha u_0''\right\}\right]\phi = 0 \tag{9}$$

with boundary conditions

$$\phi(x, -1) = \phi(x, 1) = \phi'(x, -1) = \phi'(x, 1) = 0.$$

Here, ϕ stands for the eigenfunction of disturbed stream functions, $u_0 = 1 - y^2$ and u_0'' represent the mean flow velocity profile and its second derivative, respectively. Then the stream function (ψ) is given by

$$\psi = \varepsilon\, \mathrm{Real}\{\phi(y)\, e^{i(\alpha x - \omega_R t)}\}, \tag{10}$$

and the perturbation velocities can be obtained from (10) as

$$\begin{aligned} u' &= \varepsilon\, \mathrm{Real}\{\phi'(y)\, e^{i(\alpha x - \omega_R t)}\}, \\ v' &= \varepsilon\, \mathrm{Real}\{-i\alpha\phi(y)\, e^{i(\alpha x - \omega_R t)}\}. \end{aligned} \tag{11}$$

Let

$$\begin{aligned} \phi^u(y) &= \phi_{\mathrm{R}}^u(y) + i\phi_{\mathrm{I}}^u(y) = \phi'(y), \\ \phi^v(y) &= \phi_{\mathrm{R}}^v(y) + i\phi_{\mathrm{I}}^v(y) = -i\alpha\phi(y). \end{aligned} \tag{12}$$

Then the linear solution can be written as

$$\begin{aligned} u' &= \varepsilon e^{-\alpha_I x}(\phi_{\mathrm{R}}^u \cos(\alpha_{\mathrm{R}} x - \omega_{\mathrm{R}} t) \\ &\quad - \phi_{\mathrm{I}}^u \sin(\alpha_{\mathrm{R}} x - \omega_{\mathrm{R}} t)), \\ v' &= \varepsilon e^{-\alpha_I x}(\phi_{\mathrm{R}}^v \cos(\alpha_{\mathrm{R}} x - \omega_{\mathrm{R}} t) \\ &\quad - \phi_{\mathrm{I}}^v \sin(\alpha_{\mathrm{R}} x - \omega_{\mathrm{R}} t)). \end{aligned} \tag{13}$$

The linear solution will provide an inflow boundary condition and will be used to check the accuracy of the numerical results of our tests.

The particular problem chosen here for study uses $\mathrm{Re} = 5000$ and $\omega_{\mathrm{R}} = 0.330017$. For these parameters, the Orr–Sommerfeld solution, which is obtained by a spectral method with high order Chebyshev polynomials, gives $\alpha = 1.1557 + i0.0106$ as a least-damped eigenvalue. Its eigenfunction is depicted in Fig. 2.

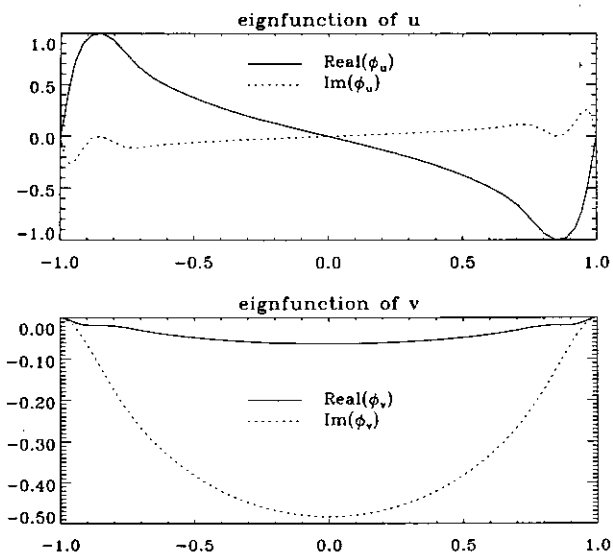

FIGURE 2.

3. GOVERNING EQUATIONS AND BOUNDARY CONDITIONS IN PERTURBATION FORM

According to (5), we can write the primitive variables in perturbation form:

$$u = u_0 + u', \qquad v = v_0 + v', \qquad P = P_0 + P'. \tag{14}$$

Substituting (14) into Eqs. (1), (2), and (3), we may rewrite the governing equations in perturbation form:

$$\begin{aligned}
&\frac{\partial u}{\partial t} + \frac{\partial u_0 u}{\partial x} + \frac{\partial uu}{\partial x} + \frac{\partial uv}{\partial y} - \frac{1}{\mathrm{Re}}\left(\frac{\partial^2 u}{\partial x^2} + \frac{\partial^2 u}{\partial y^2}\right) \\
&\qquad + v\frac{\partial u_0}{\partial y} + \frac{\partial P}{\partial x} = 0, \\
&\frac{\partial v}{\partial t} + \frac{\partial u_0 v}{\partial x} + \frac{\partial uv}{\partial x} + \frac{\partial vv}{\partial y} \\
&\qquad - \frac{1}{\mathrm{Re}}\left(\frac{\partial^2 v}{\partial x^2} + \frac{\partial^2 v}{\partial y^2}\right) + \frac{\partial P}{\partial y} = 0, \\
&\frac{\partial u}{\partial x} + \frac{\partial v}{\partial y} = 0.
\end{aligned} \tag{15}$$

Here, for simplicity, we drop the prime notation, so that u, v, and P actually now stand for the perturbation variables u', v', and P'. The boundary conditions for u and v on the solid wall are simply

$$\begin{aligned}
u(x, -1, t) = v(x, -1, t) = 0, \\
u(x, 1, t) = v(x, 1, t) = v(x, 1, t) = 0.
\end{aligned} \tag{16}$$

Since a staggered grid is used (see Fig. 3), we do not need to specify P at the solid wall where $v = 0$.

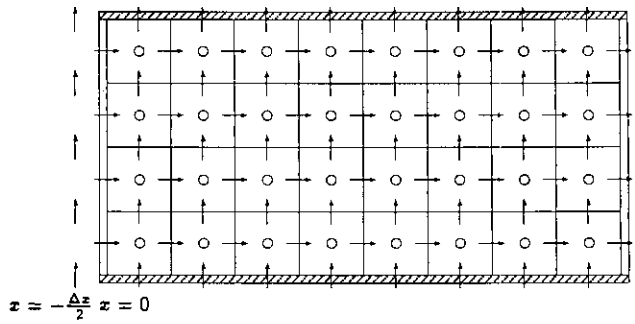

FIG. 3. Staggered grid for channel flow.

The inflow boundary condition is specified by the linear solution for the given perturbation mode. Here, the u-component is given at $x = 0$ and the v-component is given at $x = -\Delta x/2$:

$$\begin{aligned}
u(0, y, t) &= \varepsilon[\phi_{\mathrm{R}}^u \cos(\omega_{\mathrm{R}} t) + \phi_{\mathrm{I}}^u \sin(\omega_{\mathrm{R}} t)], \\
v\left(-\frac{\Delta x}{2}, y, t\right) &= \varepsilon e^{\alpha_{\mathrm{I}}(\Delta x/2)}\left[\phi_{\mathrm{R}}^v \cos\left(-\alpha_{\mathrm{R}}\frac{\Delta x}{2} - \omega_{\mathrm{R}} t\right)\right. \\
&\qquad \left. - \phi_{\mathrm{I}}^v \sin\left(-\alpha_{\mathrm{R}}\frac{\Delta x}{2} - \omega_{\mathrm{R}} t\right)\right].
\end{aligned} \tag{17}$$

The outflow boundary condition will be discussed in Section 5.

4. FOURTH-ORDER FULLY IMPLICIT FINITE DIFFERENCE SCHEME

We use a uniform staggered grid for our problem (Fig. 4). As in the earlier work, we use a second-order backward Euler difference in the time direction,

$$\frac{\partial \phi}{\partial t} = \frac{3\phi_{i,j}^{n+1} - 4\phi_{i,j}^n + \phi_{i,j}^{n-1}}{2\Delta t} + O(\Delta t^2),$$

where, ϕ stands for generic variables.

To minimize the possible phase errors and to achieve higher accuracy, a fourth-order central difference in space is applied to discretize (15). Using

$$\left.\frac{\partial \phi}{\partial x}\right|_i = \frac{-\phi_{i+2} + 8\phi_{i+1} - 8\phi_{i-1} + \phi_{i-2}}{12\Delta x} + O(\Delta x^4), \tag{18}$$

$$\begin{aligned}
\left.\frac{\partial^2 \phi}{\partial x^2}\right|_i &= \frac{-\phi_{i+2} + 16\phi_{i+1} - 30\phi_i + 16\phi_{i-1} - \phi_{i-2}}{12\Delta x^2} \\
&\qquad + O(\Delta x^4),
\end{aligned} \tag{19}$$

$$\begin{aligned}
\left.\frac{\partial \phi}{\partial x}\right|_{i+1/2} &= \frac{-\phi_{i+2} + 27\phi_{i+1} - 27\phi_i + \phi_{i-1}}{24\Delta x} \\
&\qquad + O(\Delta x^4)
\end{aligned} \tag{20}$$

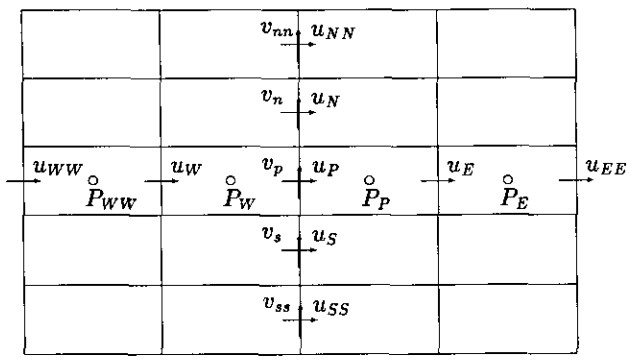

FIG. 4. Neighbor points for u-equation.

to discretize all spatial terms in (15), we obtain the difference scheme written in general form:

$$A_{EE}u_{EE}+A_Eu_E+A_Wu_W+A_{WW}u_{WW}+A_{NN}u_{NN}+A_Nu_N+A_Su_S+A_{SS}u_{SS}-A_Pu_P+C_{WW}P_{WW}+C_WP_W+C_EP_E-C_PP_P=Su, \tag{21}$$

$$B_{EE}v_{EE}+B_Ev_E+B_Wu_W+B_{WW}v_{WW}+B_{NN}v_{NN}+B_Nv_N+B_Sv_S+B_{SS}v_{SS}-B_Pv_P+D_{SS}P_{SS}+D_SP_S+D_NP_N-D_PP_P=Sv, \tag{22}$$

$$F_{EE}u_{EE}+F_Eu_E+F_Wu_W-F_Pu_P+G_{NN}v_{NN}+G_Nv_N+G_Sv_S-G_Pv_P=Sm. \tag{23}$$

Here,

$$u_{EE}=u_{i+2,j},$$
$$u_E=u_{i+1,j},$$
$$u_W=u_{i-1,j},$$
$$u_{WW}=u_{i-2,j},$$

and similarly for v and P. Thus,

$$A_{EE}=-\frac{1}{12\mathrm{Re}\,\Delta x^2}+\frac{1}{12\Delta x}(u_{i+2,j}+u_{0i,j}),$$
$$A_E=\frac{4}{3\mathrm{Re}\,\Delta x^2}-\frac{2}{3\Delta x}(u_{i+1,j}+u_{0i,j}),$$
$$A_W=\frac{4}{3\mathrm{Re}\,\Delta x^2}+\frac{2}{3\Delta x}(u_{i-1,j}+u_{0i,j}),$$
$$A_{WW}=-\frac{1}{12\mathrm{Re}\,\Delta x^2}-\frac{1}{12\Delta x}(u_{i-2,j}+u_{0i,j}),$$
$$A_{NN}=-\frac{1}{\mathrm{Re}}\frac{1}{12\Delta y^2}+\frac{1}{12\Delta y}v_{nn},$$
$$A_N=\frac{1}{\mathrm{Re}}\frac{4}{3\Delta y^2}-\frac{2}{3\Delta y}v_n,$$
$$A_S=\frac{1}{\mathrm{Re}}\frac{4}{3\Delta y^2}+\frac{2}{3\Delta y}v_s,$$
$$A_{SS}=-\frac{1}{\mathrm{Re}}\frac{1}{12\Delta y^2}-\frac{1}{12\Delta y}v_{ss},$$
$$A_P=\frac{3}{2\Delta t}+\frac{5}{2\mathrm{Re}}\left(\frac{1}{\Delta x^2}+\frac{1}{\Delta y^2}\right),$$
$$C_E=\frac{1}{24\Delta x},$$
$$C_W=C_P=\frac{27}{24\Delta x},$$
$$C_{WW}=-\frac{1}{24\Delta x},$$
$$Su=\frac{-4u_{i,j}^n+u_{i,j}^{n-1}}{2\Delta t}-2y_jv_p. \tag{24}$$

Here, the lower case subscripts denote the approximate value of v at the points associated with u, which need to be evaluated by high-order interpolation (see Fig. 5). For the interior points ($4<j<nj-3$):

$$\begin{aligned}
v_{nn}&=(9(v_{i,j+2}+v_{i,j+3}+v_{i-1,j+3}+v_{i-1,j+2})\\
&\quad-(v_{i-2,j+1}+v_{i-2,j+4}+v_{i+1,j+1}+v_{i+1,j+4}))/32,\\
v_n&=(9(v_{i,j+1}+v_{i,j+2}+v_{i-1,j+2}+v_{i-1,j+1})\\
&\quad-(v_{i-2,j}+v_{i-2,j+3}+v_{i+1,j}+v_{i+1,j+3}))/32,\\
v_p&=(9(v_{i,j}+v_{i,j+1}+v_{i-1,j+1}+v_{i-1,j})\\
&\quad-(v_{i-2,j-1}+v_{i-2,j+2}+v_{i+1,j-1}+v_{i+1,j+2}))/32,\\
v_s&=(9(v_{i,j-1}+v_{i,j}+v_{i-1,j}+v_{i-1,j-1})\\
&\quad-(v_{i-2,j-2}+v_{i-2,j+1}+v_{i+1,j-2}+v_{i+1,j+1}))/32,\\
v_{ss}&=(9(v_{i,j-2}+v_{i,j-1}+v_{i-1,j-1}+v_{i-1,j-2})\\
&\quad-(v_{i-2,j-3}+v_{i-2,j}+v_{i+1,j-3}+v_{i+1,j}))/32.
\end{aligned} \tag{25}$$

We need special treatment when $j=nj-3$ or $j=4$.

On the solid wall boundary, we change the y-direction difference to second order and maintain fourth order in the x-direction. Then, the truncation error is $O(\Delta x^4+\Delta y^2)$.

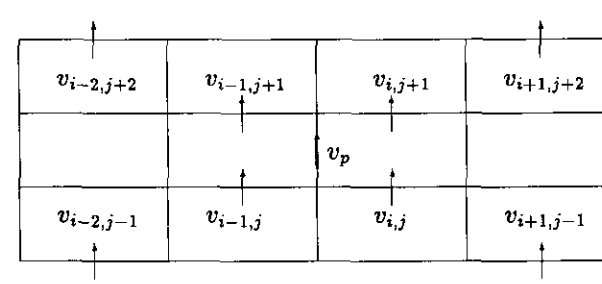

FIG. 5. Fourth-order approximation for v at a u point (interior points).

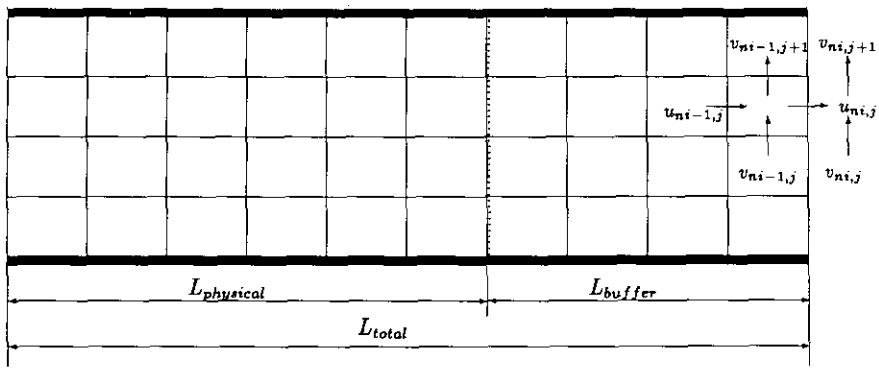

FIG. 6. Outflow boundary conditions.

5. OUTFLOW BOUNDARY TREATMENT

To avoid reflection of the outgoing waves, we use the so-called buffer domain, which is added at the outflow boundary. Thus, the whole domain contains two parts, the physical domain and the buffer domain (Fig. 6).

Let b and b_{Re} denote the buffer functions for velocities and the Reynolds number, respectively. The governing equations can then be rewritten as

$$\frac{\partial u}{\partial t}+\frac{\partial u_0 u}{\partial x}+v\frac{\partial u_0}{\partial y}+\frac{\partial uu}{\partial x}+\frac{\partial uv}{\partial y} -\frac{b_{\mathrm{Re}}}{\mathrm{Re}}\left(b\frac{\partial^2 u}{\partial x^2}+\frac{\partial^2 u}{\partial y^2}\right)+\frac{\partial P}{\partial x}=0, \tag{26}$$

$$\frac{\partial v}{\partial t}+\frac{\partial u_0 v}{\partial x}+\frac{\partial uv}{\partial x}+\frac{\partial vv}{\partial y} -\frac{b_{\mathrm{Re}}}{\mathrm{Re}}\left(b\frac{\partial^2 v}{\partial x^2}+\frac{\partial^2 v}{\partial y^2}\right)+\frac{\partial P}{\partial y}=0, \tag{27}$$

$$\frac{\partial u}{\partial x}+\frac{\partial v}{\partial y}=0, \tag{28}$$

where

$$b(x)=\begin{cases}\dfrac{\tanh(L_{\mathrm{total}}-x)}{\tanh(L_{\mathrm{buffer}})}, & L_{\mathrm{physical}}\leqslant x\leqslant L_{\mathrm{total}},\\ 1, & 0\leqslant x\leqslant L_{\mathrm{physical}};\end{cases}$$

$$b_{\mathrm{Re}}(x)=\begin{cases}\dfrac{49}{L_{\mathrm{buffer}}^2}(x-L_{\mathrm{physical}})^2+1, & L_{\mathrm{physical}}\leqslant x\leqslant L_{\mathrm{total}},\\ 1, & 0\leqslant x\leqslant L_{\mathrm{physical}}.\end{cases}$$

Note that the solution in the buffer domain is not consistent with the physics and that, for efficiency, the buffer domain should be as short as possible.

A successful treatment for the outflow boundary points has been developed on staggered grids, which only needs a very small buffer domain, in fact, shorter than one T-S wavelength. The treatment may be described in two steps (Fig. 6):

1. Update $u_{ni,j}$ by equations of mass conservation after each relaxation

$$u_{ni,j}^{n+1}=u_{ni-1,j}^{n}-\frac{v_{ni-1,j+1}^{n}-v_{ni-1,j}^{n}}{\Delta y}\cdot\Delta x. \tag{29}$$

2. Update $v_{ni,j}$ by the assumption that

$$\frac{\partial^2 v}{\partial x^2}=0 \qquad \text{or} \qquad v_{ni,j}^{n+1}=2v_{ni-1,j}^{n}-v_{ni-2,j}^{n}. \tag{30}$$

6. LINE DISTRIBUTIVE RELAXATION

The discretization of the time-dependent incompressible equations (1)–(3) may be written in brief as

$$\begin{aligned}Q_{\tau h}u+\delta_x P&=0,\\ Q_{\tau h}v+\delta_y P&=0,\\ \delta_x u+\delta_y v&=0,\end{aligned} \tag{31}$$

where $Q_{\tau h}=\delta_\tau^- +\tilde{u}\delta_x+\tilde{v}\delta y-(1/\mathrm{Re})\,\Delta_h$, δ_τ^- is the backward difference operator, δ_x and δ_y are central difference operators, and Δ_h is a discrete Laplacian. We rewrite (31) in matrix form:

$$\begin{bmatrix}Q_{\tau h} & 0 & \delta_x\\ 0 & Q_{\tau h} & \delta_y\\ \delta_x & \delta_y & 0\end{bmatrix}\begin{bmatrix}u\\ v\\ P\end{bmatrix}=\begin{bmatrix}f1\\ f2\\ f3\end{bmatrix}. \tag{32}$$

The problem with system (32) is that the third equation causes trouble for conventional iterative solvers, which

usually fail to converge due to lack of matrix diagonal dominance. The basic idea behind distributive relaxation is to introduce a preconditioner to improve (32). To explain this, we use new variables, $w1$, $w2$, and $w3$, defined by the relation

$$\begin{bmatrix} u \\ v \\ p \end{bmatrix} = M \begin{bmatrix} w1 \\ w2 \\ w3 \end{bmatrix} = \begin{bmatrix} 1 & 0 & -\delta_x \\ 0 & 1 & -\delta_y \\ 0 & 0 & Q_{\tau h} \end{bmatrix} \begin{bmatrix} w1 \\ w2 \\ w3 \end{bmatrix}; \quad (33)$$

then, applying the relation to (32) yields

$$\begin{bmatrix} Q_{\tau h} & 0 & \delta_x \\ 0 & Q_{\tau h} & \delta_y \\ \delta_x & \delta_y & 0 \end{bmatrix} \begin{bmatrix} u \\ v \\ P \end{bmatrix} = \begin{bmatrix} Q_{\tau h} & 0 & \delta_x \\ 0 & Q_{\tau h} & \delta_y \\ \delta_x & \delta_y & 0 \end{bmatrix} \begin{bmatrix} 1 & 0 & -\delta_x \\ 0 & 1 & -\delta_y \\ 0 & 0 & Q_{\tau h} \end{bmatrix} \begin{bmatrix} w1 \\ w2 \\ w3 \end{bmatrix}. \quad (34)$$

Thus, (34) is related to the linear system

$$\begin{bmatrix} Q_{\tau h} & 0 & 0 \\ 0 & Q_{\tau h} & 0 \\ \delta_x & \delta_y & -\Delta_h \end{bmatrix} \begin{bmatrix} w1 \\ w2 \\ w3 \end{bmatrix} = \begin{bmatrix} f1 \\ f2 \\ f3 \end{bmatrix}. \quad (35)$$

The point here is that (35) is easily solved by conventional iterative methods. However, the traditional distributive relaxation works very well for isotropic problems, but meets difficulties in the presence of anisotropy. For our applications, $\Delta y \ll \Delta x$, which yields extreme anisotropy, and the convergence properties of standard distributive relaxation quickly degenerate. A line distributive relaxation scheme has been developed in this work which successfully overcomes the difficulty with anisotropic grids. Consider the original system,

$$A_E u_E + A_W u_W + A_N u_N + A_S u_S - A_P u_P + \frac{P_W - P_P}{\Delta x} = Su, \quad (36)$$

$$B_E v_E + B_W v_W + B_N v_N + B_S v_S - B_P v_P + \frac{P_S - P_P}{\Delta y} = Sv, \quad (37)$$

$$\frac{u_E - u_P}{\Delta x} + \frac{v_N - v_P}{\Delta y} = Sm; \quad (38)$$

the procedure for a y-line distributive relaxations can be described as follows:

1. Freezing P, perform y-line Gauss–Seidel relaxation on (36) to obtain a new u.

2. Freezing P, perform y-line Gauss–Seidel relaxation on (37) to obtain a new v.

3. For all grid cells (Fig. 7) on each y-line in term, modify all velocities simultaneously to satisfy the continuity equations. Referring to Fig. 7, we have

$$\frac{(u_E^{\mathrm{I}} + \beta\delta_1) - (u_W^{\mathrm{I}} - \beta\delta_1)}{\Delta x} + \frac{(v^{\mathrm{II}} + \delta_1 - \delta_2) - v^{\mathrm{I}}}{\Delta y} = Sm^{\mathrm{I}} \quad (39)$$

in cell I. Similarly, we have five equations corresponding to the continuity equation on five neighboring cells. The five unknowns, $\delta_1, \delta_2, \delta_3, \delta_4$, and δ_5 are thus determined by this system. The u and v are then updated on all five cells:

$$\begin{aligned} u_E^{\mathrm{I}} &\leftarrow u_E^{\mathrm{I}} + \beta\delta_1, \\ u_W^{\mathrm{I}} &\leftarrow u_W^{\mathrm{I}} - \beta\delta_1, \\ v^{\mathrm{II}} &\leftarrow v^{\mathrm{II}} + \delta_1 - \delta_2, \\ &\vdots \end{aligned} \quad (40)$$

4. Modify the pressure in each cell in turn to satisfy the momentum equation. In cell I, modify P_{I} by using the x-momentum equation:

$$P_{\mathrm{I}} \leftarrow P_{\mathrm{I}} + \delta P_{\mathrm{I}}, \quad (41)$$

where

$$\delta P_{\mathrm{I}} = \frac{(A_P + A_E)\,\beta\delta_1}{C_P}.$$

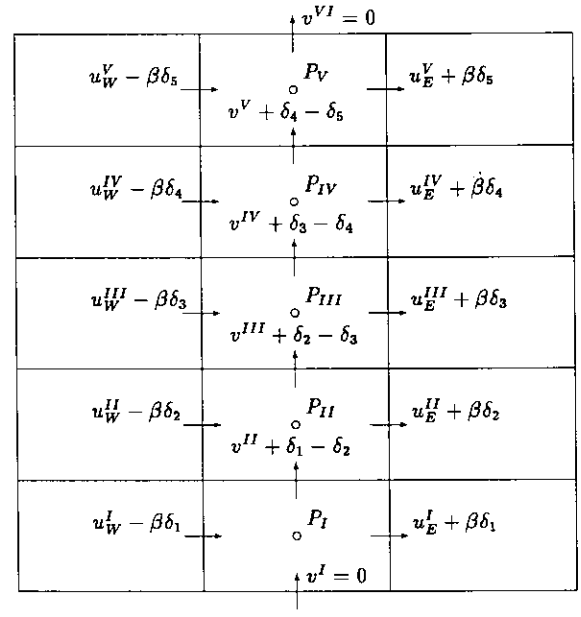

FIG. 7. Line distributive relaxation.

In cell II, modify P_{II} by using the y-momentum equation:

$$P_{II} \leftarrow P_{II} + \delta P_{II}, \tag{42}$$

where

$$\delta P_{II} = \frac{B_P(\delta_1 - \delta_2)}{D_P} + \delta P_I.$$

The modification at other points is given by

$$P_j \leftarrow P_j + \delta P_j, \tag{43}$$

where

$$\delta P_j = \frac{B_P(\delta_{j-1} - \delta_j)}{D_P} + \delta P_{j-1}, \qquad j = 2, 3, 4, 5.$$

7. SEMI-COARSENING MULTIGRID ALGORITHM

To solve the large scale discrete system that arises at each time step from the fully implicit time-marching scheme, conventional relaxation methods are much too inefficient. To obtain optimal efficiency, we use a multigrid scheme based on distributive relaxation. Because of the high degree of anisotropy caused by our grids, a semi-coarsening scheme (coarsening in y-direction only, see Fig. 8) is applied. In Fig. 8, u^h, v^h, and P^h represent values of fine grid points and u^{2h}, v^{2h}, and P^{2h} represent values of coarse grid points.

For simplicity of discussion, we consider only the two grid case as depicted in Fig. 8. We use a full approximation scheme (FAS) to accommodate nonlinearities. A two-level FAS algorithm for an equation of the form

$$L_h u_h = f_h$$

may be described loosely as follows:

(i) relax on $L_h u_h = f_h$,

(ii) solve $L_{2h} u_{2h} = L_{2h} I_h^{2h} u_h + \bar{I}_h^{2h}(f_h - L_h u_h)$,

(iii) replace $u_h \leftarrow u_h + I_{2h}^h(u_{2h} - I_h^{2h} u_h)$.

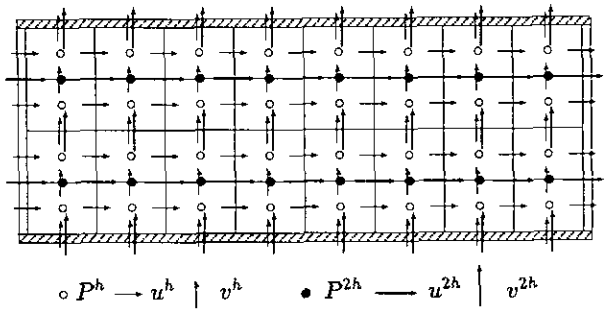

FIG. 8. Two-level staggered grid.

The notation we have introduced includes the difference operators L_h and L_{2h}, the restriction operators I_h^{2h} (for the approximation) and $\bar{I}_h^{2h}$ (for the residual), and the interpolation operator I_{2h}^h. We describe these symbols in more detail as follows.

Relaxation on the coarse grid requires restriction of the approximation and residual from the fine grid to the coarser grid to provide initial guesses and right-hand sides, respectively. For restriction of the approximation, we use the stencils

$$I_h^{2h}(u): \begin{bmatrix} \frac{1}{2} \\ \frac{1}{2} \end{bmatrix},$$

$$I_h^{2h}(v): \begin{bmatrix} 0 \\ 1 \\ 0 \end{bmatrix},$$

$$I_h^{2h}(P): \begin{bmatrix} \frac{1}{2} \\ \frac{1}{2} \end{bmatrix}.$$

For restriction of residuals, we use the following full-weighting stencils for semi-coarsening grids, which come from the so-called area law developed in [7]. Let Ru, Rv, and Rm denote the residual of x-momentum, y-momentum, and continuity equations, respectively; we obtain

$$I_h^{2h}(Ru): \begin{bmatrix} \frac{1}{2} \\ \frac{1}{2} \end{bmatrix},$$

$$I_h^{2h}(Rv): \begin{bmatrix} \frac{1}{4} \\ \frac{1}{2} \\ \frac{1}{4} \end{bmatrix},$$

$$I_h^{2h}(Rm): \begin{bmatrix} \frac{1}{2} \\ \frac{1}{2} \end{bmatrix}.$$

After relaxation on the coarse grid, we interpolate the corrections from the coarse grid up to the fine grid:

$$\begin{aligned} u_h &\leftarrow u_h + I_{2h}^h(u)(u_{2h} - I_h^{2h}(u)\, u_h), \\ v_h &\leftarrow v_h + I_{2h}^h(v)(v_{2h} - I_h^{2h}(v)\, v_h), \\ P_h &\leftarrow P_h + I_{2h}^h(P)(P_{2h} - I_h^{2h}(P)\, P_h). \end{aligned} \tag{44}$$

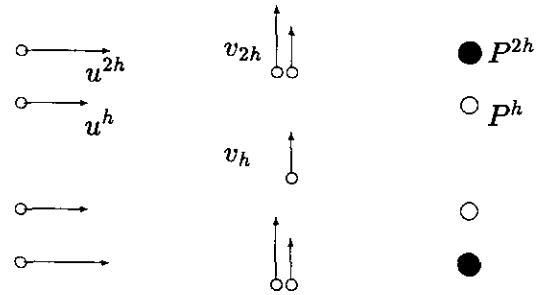

FIG. 9. Bilinear interpolation for u, v, and P.

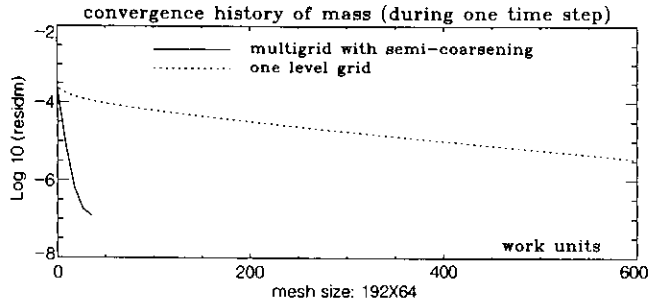

FIG. 10. Convergence history of semi-coarsening multigrid method.

Here we use bilinear interpolation, given by the following stencil (Fig. 9):

$$I_{2h}^{h}(u): \begin{bmatrix} \frac{3}{4} \\ \frac{1}{4} \end{bmatrix} \quad \text{and} \quad \begin{bmatrix} \frac{1}{4} \\ \frac{3}{4} \end{bmatrix},$$

$$I_{2h}^{h}(v): \begin{bmatrix} 0 \\ 1 \\ 0 \end{bmatrix} \quad \text{and} \quad \begin{bmatrix} \frac{1}{2} \\ \frac{1}{2} \end{bmatrix},$$

$$I_{2h}^{h}(P): \begin{bmatrix} \frac{3}{4} \\ \frac{1}{4} \end{bmatrix} \quad \text{and} \quad \begin{bmatrix} \frac{1}{4} \\ \frac{3}{4} \end{bmatrix}.$$

Both semi-coarsening and line distributive relaxation can handle anisotropy effectively when the weaker directions are known. However, when these directions are unknown, semi-coarsening in one direction coupled with line distributive relaxation in the other direction is more robust, and it is able to achieve optimal multigrid efficiency for general cases of anisotropy.

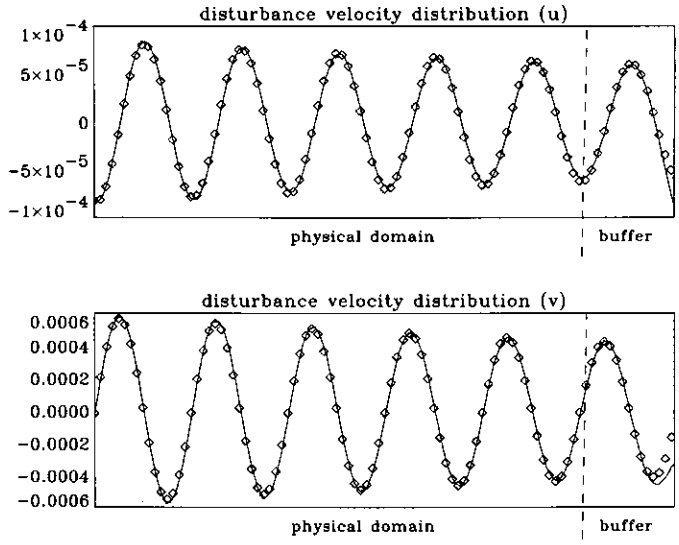

FIG. 11. Comparison of the numerical and theoretical solutions at $t = 12T$: ——— numerical solution; ◇ theoretical solution; computational domain: 5 T-S wavelength physical + 1 wavelength buffer; grids: 192×64; scheme: fourth-order finite difference.

8. COMPUTATIONAL RESULTS

Let $\mathrm{Re} = 5000$ and $\omega = 0.33017$. For these parameters, the Orr–Sommerfeld solution gives $\alpha = 1.1557 + i0.0106$. The perturbation amplitude is set to $\varepsilon = 1.2 \times 10^{-3}$. The channel length is set to five Tollmien–Schlichting (T-S) wavelengths and one wavelength buffer domain is added to the rear of the channel. Thus, the total length of the computational domain is six T-S wavelengths. The grid used in this work

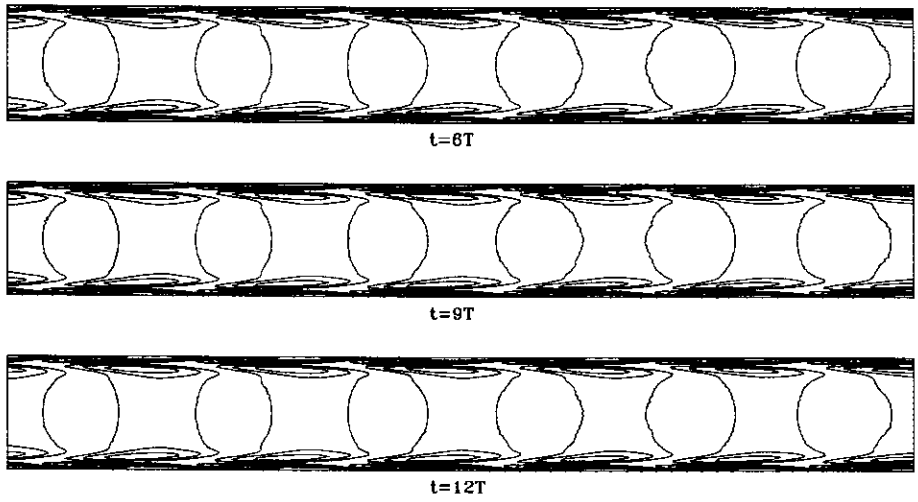

FIG. 12. Disturbance vorticity contours for the first three T-S wavelengths of the physical domain; contour intervals = 10^{-3}.

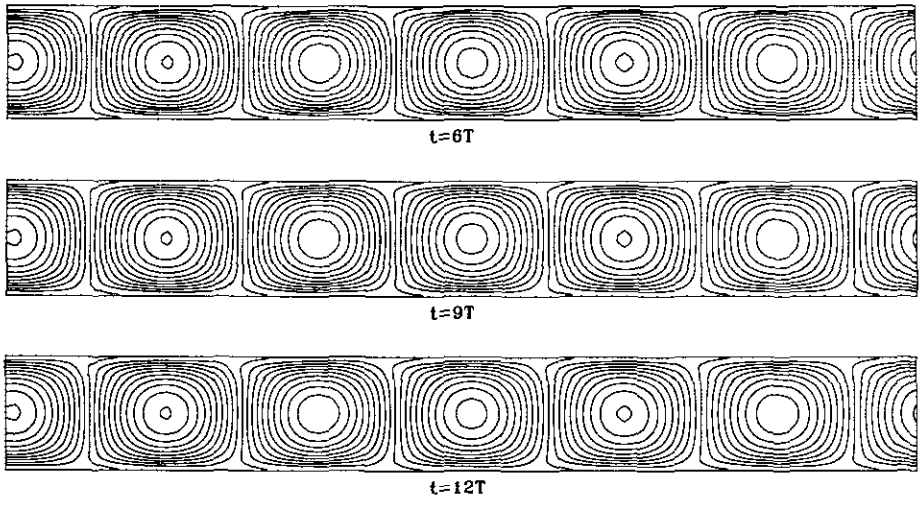

FIG. 13. Disturbance streamfunction contours for the first three T-S wavelengths of the physical domain; contour intervals = 5×10^{-5}.

is 192×64. Therefore, the grid for each T-S wavelength is 32×64. The grid is anisotropic with $\Delta x \equiv 0.1699 \gg \Delta y \equiv 0.03125$. To examine the efficiency of semi-coarsening multigrid, a comparison of the convergence histories of multigrid and single-grid relaxation at one time step is depicted in Fig. 10. The code requires about 36 μs per physical grid point per time step on the CRAY-YMP and about 70 μs on the CRAY2 at NASA/Langley Research Center. This is comparable to [8], which requires about 100 μs per physical grid point per time step on CRAY2.

Figure 10 shows the convergence rate of the semi-coarsening multigrid method, which is about 0.04 per $V(2, 2)$ cycle, much better than the depicted performance of single-grid relaxation. The streamwise and the normal components, u and v, of the perturbation velocity after 12 T-S periods are compared with the theoretical solution given by the linear theory at a vertical position close to the lower wall ($y = -0.125$ for v and $y = -0.119375$ for u), see Figs. 11a and b, respectively. The excellent agreement in both amplitude and phase between our computational results and the theoretical solution was observed in the physical domain. The relative L_2 norms for both u and v (defined as $\|u - \hat{u}\|_2 / \|\hat{u}\|_2$ and $\|v - \hat{v}\|_2 / \|\hat{v}\|_2$, respectively, where u and v are numerical solutions, and $\hat{u}$ and $\hat{v}$ are theoretical solutions) in the physical domain are 0.063 and 0.061, respectively, for the 192×64 grid. Figures 12 and 13 give the distribution of the respective disturbance vorticity and streamfunction at different times, showing that no reflection was observed in the physical domain. The results are, of course, poor near the outflow boundary, but they are located in the buffer domain and therefore are ignorable.

9. CONCLUDING REMARKS

- The fourth-order and fully implicit time-marching scheme on a staggered grid is highly accurate for spatially evolving problems.
- Semi-coarsening multigrid and line distributive relaxation is very efficient, with a convergence rate of about 0.04 per $V(2, 2)$ cycle, even in the presence of strong anisotropy.
- The outflow boundary condition proposed here for staggered grids successfully minimizes the length of the buffer domain and eliminates wave reflection.

ACKNOWLEDGMENTS

The authors thank Dr. Steve McCormick, at the University of Colorado at Denver and Drs. Tom Zang, Craig Streett, and Ron Joslin at NASA Langley Research Center for their guidance and helpful discussions.

REFERENCES

1. L. Kleiser and T. A. Zang, *Ann. Rev. Fluid Mech.* **23**, 495 (1991).
2. C. Liu, Z. Liu, and S. McCormick, *Comput. Phys. Commun.* **65**, 188 (1991).
3. C. Liu, Z. Liu, and S. McCormick, *J. Comput. Appl. Math.* **38**, 283 (1991).
4. Z. Liu, C. Liu, and S. McCormick, in *Proc. 4th Int'l Symp. CFD*, 1991, pp. 705–710.
5. C. L. Streett and M. G. Macaraeg, *Appl. Numer. Math.* **6**, 123 (1989).
6. A. Brandt, *Multigrid Techniques: Guide with Application to Fluid Dynamics*, GMD Studie, GMD, St. Augustine, 1984.
7. C. Liu, Ph.D. thesis, University of Colorado at Denver, 1989.
8. G. Danabasoglu, A. Saati, and S. Biringen, in *Proceedings, 1st Int'l Conference on Computational Physics, 1990*, pp. 312–315.